Biophysical Journal, Volume *115*

Supplemental Information

Hydrophobic Mismatch Modulates Stability and Plasticity of Human Mitochondrial VDAC2

Shashank Ranjan Srivastava, Punit Zadafiya, and Radhakrishnan Mahalakshmi

SUPPORTING METHODS

Indirect folding in phosphocholine bicelles

Folding of hVDAC2 in 20 mM DPC micelles was initiated by 10-fold dilution of the unfolded protein stock in DPC micelles prepared in buffer A containing 10 mM DTT, at 4 °C. The sample was gently mixed for 5-6 h at 4 °C and trace amounts of aggregated protein was removed by centrifugation. The final folded protein concentration in 20 mM DPC micelles was 50 μM. This served as the 10X folded protein-DPC stock. Empty bicelles of various q in 0.9 volume buffer A were prepared by mixing specific stock concentrations (to achieve 4 mM final concentrations) of the long chain lipid with 2 mM (final concentration) DPC. The mixture was subjected to repeated freeze-thaw cycles using liquid nitrogen and heating, till the solution became transparent. The bicelles were chilled on ice, and 0.1 volume of the folded protein-DPC stock was diluted 10-fold in the bicelle preparation. This provided final concentrations of 5 μM protein, 4 mM DPC and 4 mM long chain lipid (bicelle q = 1.0), in buffer A containing 2 mM DTT. The reconstituted bicelles were subjected to three rounds of heating (35 °C) – cooling (4 °C) – vortexing (30 s) cycles and then allowed to equilibrate overnight at 4 °C by gentle mixing at 15 rpm. Trace amounts of aggregated protein was removed by centrifugation.

SUPPORTING TABLES

Table S1. Temperatures used for simulation according to the lipid system

Lipid	Phase transition temperature	Temperature for simulations	Thickness (hydrocarbon region)[@]	Thickness (bilayer)[@]
DMPC	24 °C	25 °C (298 K)	~25.7 Å	~37.0 Å
DPPC	41 °C	42 °C (315 K)	~28.5 Å	~40.0 Å
DSPC	55 °C	56 °C (329 K)	~32.0 Å	~43.0 Å
DPPC/DSPC	-	47.5 °C (320.5 K) [#]		
Cholesterol + DPPC	-	42 °C (315 K)		

[#]Numerical average of the phase transition temperatures of DPPC and DSPC was used.
[@]Obtained from Ref. (1).

Table S2. Cholesterol-doped lipidic bicelles.

Bicelle	% Cholesterol[#,$]		
	0.02%	**0.03%**	**0.04%**
DMPC/DPC	1.0	1.0	1.0
DPPC/DPC	1.0	1.0	1.0
DSPC/DPC	1.0	–	–

[#]Bicelle *q* that could be prepared is indicated.
[$]Cholesterol percentage calculation: The number of moles of the long chain lipid for $q = 1$ was first derived. The number of moles of cholesterol that would constitute x% was then calculated, with respect to mole amounts of the long chain lipid. This was then converted to milligram amounts of cholesterol to be added in the solution. This milligram amount was represented as percent w/v of cholesterol in the final solution.

SUPPORTING FIGURES

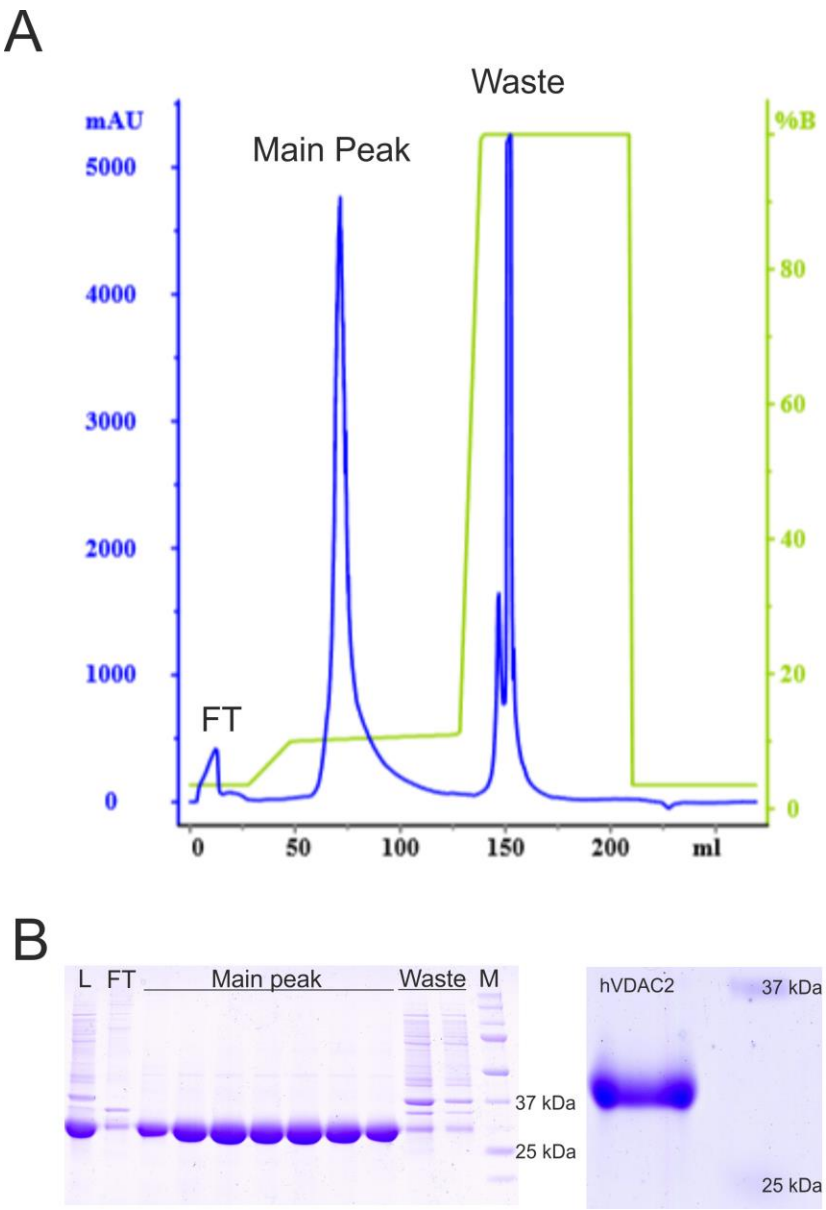

Figure S1. hVDAC2 purification. (A) Representative denaturing fast protein liquid chromatography (FPLC) purification profile of hVDAC2 obtained on a 20 ml HiPrep Q-FF column (GE Healthcare) using Buffer A (20 mM Tris-HCl pH 9.5 containing 8M urea) and Buffer B (Buffer A + 1 M NaCl). Absorbance recorded at 280 nm (blue) and the NaCl concentration gradient (green) are indicated. hVDAC2 eluted at 10-11% NaCl (main peak). (B, left) 12% SDS-PAGE gel showing protein contents of various fractions (L: load; FT: unbound flow through; Waste: tightly bound fraction; M: molecular weight marker). (B, right) Representative 12% SDS-PAGE image of purified hVDAC2 used for various experiments on the left lane with the molecular weight marker on the right. The expected MW of hVDAC2 is ~31.5 kDa.

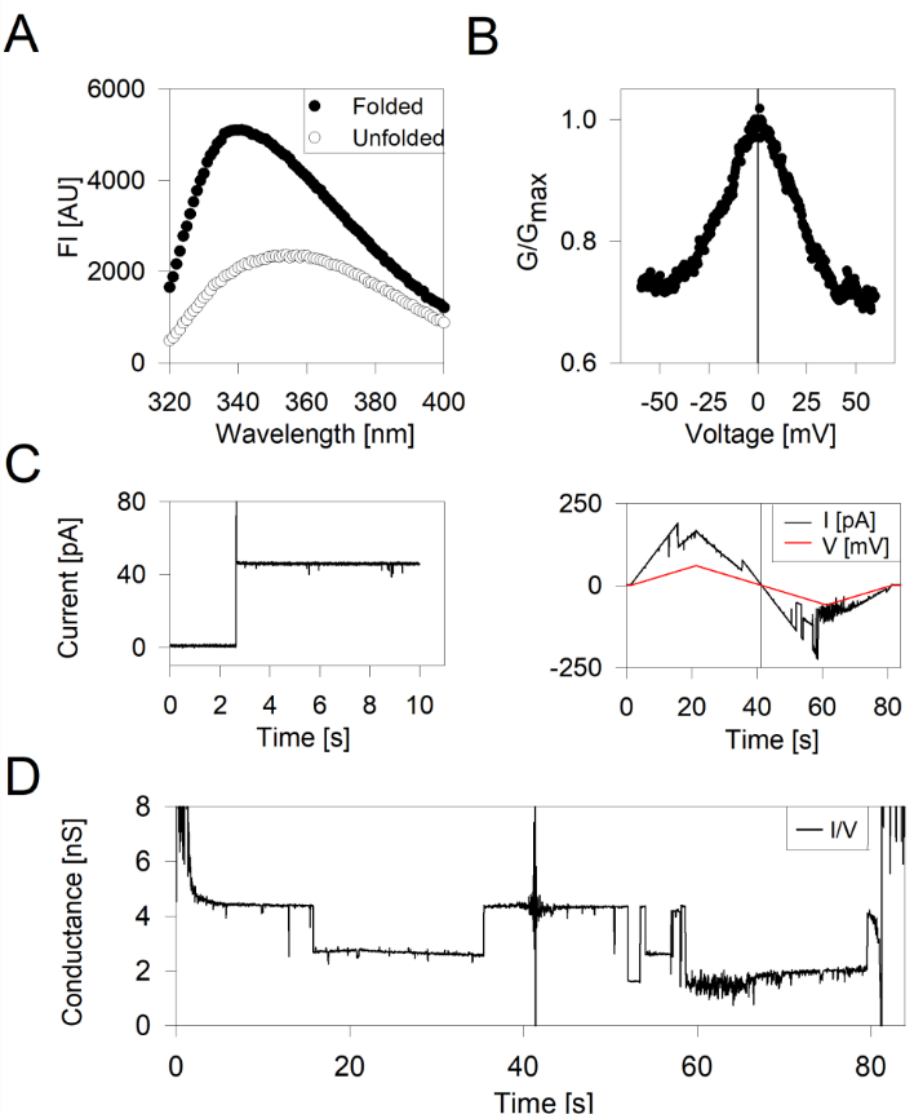

Figure S2. Characterization of folded hVDAC2. (A) Representative of tryptophan fluorescence emission spectra of folded hVDAC2 (filled black circles) and unfolded spectra (open circles) in bicelles obtained at low and high GdnHCl concentrations, respectively. The fluorescence intensity (FI) of folded hVDAC2 is high and shows a prominent blue shift when compared to unfolded hVDAC2. This data suggests that hVDAC2 is folding properly in bicelles. (B-D) Electrophysiology measurements of hVDAC2 folded in lauryldimethylamine oxide micelles and inserted in a single DiPhPC bilayer membrane containing 0.1% cholesterol (2, 3). (B) G/G_{max} plot shown for hVDAC2 protein obtained in response to a voltage gradient ranging from +60 to -60 mV is characteristic of a functional hVDAC molecule. (C, left) Single channel insertion at 10 mV produces a current of ~40 pA for the open state of hVDAC2 (2, 3). (C, right) The corresponding current measured for a voltage ramp program run from +60 mV to –60 mV with a 3mV/s ramp rate is shown. (D) Single channel conductance obtained by calculating I/V. A typical channel behavior characteristic of functional VDAC is obtained, confirming that the protein is well folded and functional in the bilayer.

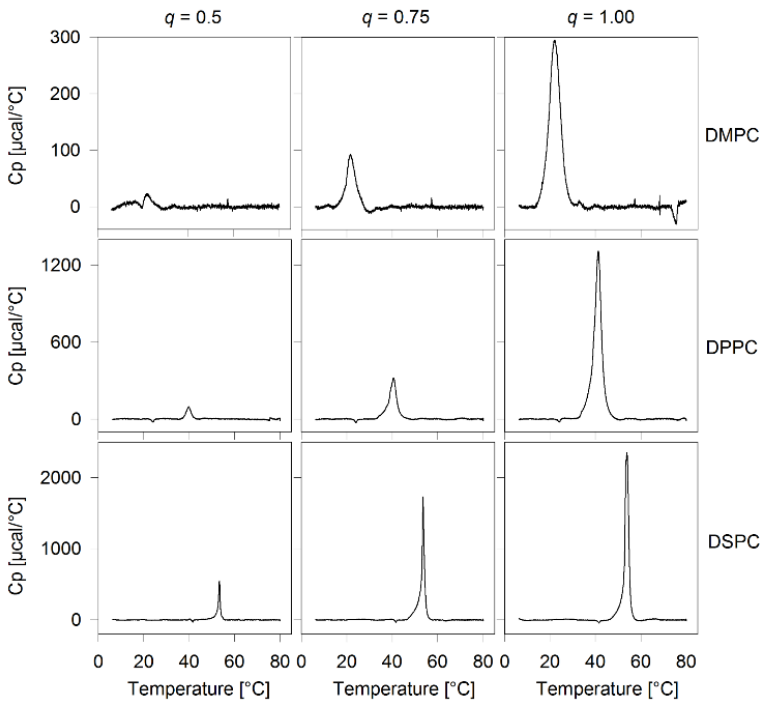

Figure S3. Comparison of bicelle phase transition temperatures using DSC. The phase transition temperature (T_m) of different lipidic bicelles (DMPC/DPC, DPPC/DPC, and DSPC/DPC) of various q was derived using differential scanning microcalorimetry (DSC). The phase transition temperature (T_m) is in excellent agreement with reported values for lipidic bicelles (4). The observation of a single transition represents homogeneous population of bicelles in all preparations.

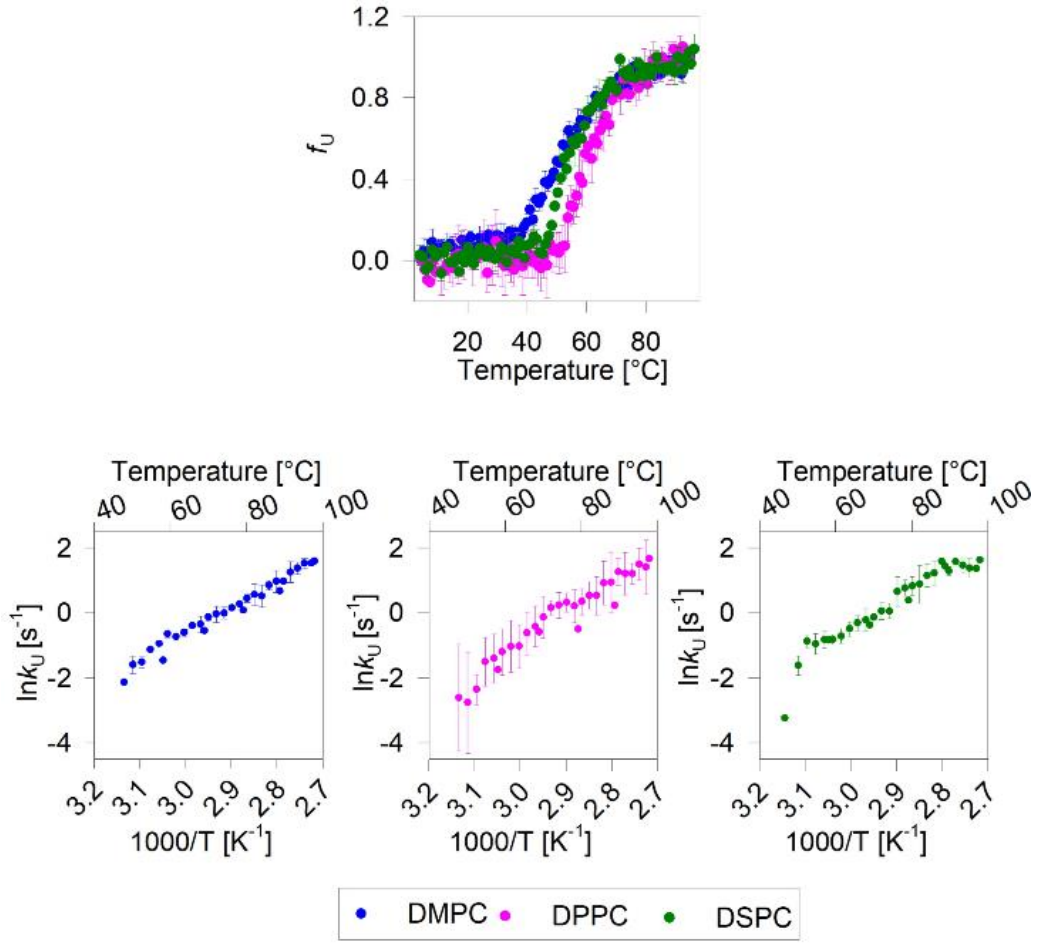

Figure S4. Effect of lipid chain length on the thermal stability of hVDAC2. (Top) Dependence of the unfolded protein fraction (f_U) on temperature, derived from far-UV CD thermal unfolding at 215 nm. Plot shows the normalized CD data obtained from q = 1.00 DMPC/DPC (blue), DPPC/DPC (pink) and DSPC/DPC (green) bicelle conditions. Error bars represent the s. d. calculated from 3-5 independent experiments. The thermal parameters presented in Figure 2B were derived from fits of individual data to the two-state thermal denaturation model. (Bottom panel) Unfolding rates (k_U) derived from fits of the isothermal unfolding kinetics to a single exponential function. Shown here is the Arrhenius plot for q = 1.0 bicelles in all three lipidic conditions. Error bars represent the s. d. calculated from 2-3 independent experiments. Activation energy (E_{act}) calculation was done by fitting the linear zone of the unfolding rates to the Arrhenius equation. Data in the regions below ~50 °C and above ~90 °C were not included in the fitting. The E_{act} presented in Figure 2D was calculated by fitting individual datasets (and not the mean data) to the Arrhenius equation. The error bars shown in Figure 2D therefore represent the s. d. obtained from the independent datasets. The k_U data clearly indicate that there are only marginal differences in E_{act} across the three lipid conditions. Color guide for both the plots is shown below the plot.

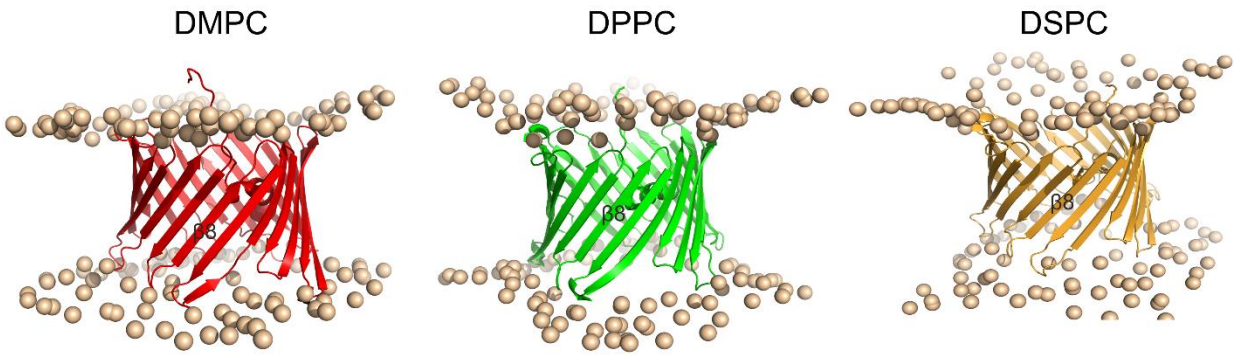

Figure S5. Increasing diacyl PC chain length increases the negative mismatch on the hVDAC2 barrel. Ribbon diagrams representing the average simulated assembly of hVDAC2 in PC lipids of varying chain length DMPC (*di*14:0-PC) (left), DPPC (*di*16:0-PC) (middle), and DSPC (*di*18:0-PC) (right). Wheat color spheres represent phosphate atom of the lipid head group. DMPC shows an excellent match to the hVDAC2 barrel, while the DSPC bilayer shows the highest negative mismatch with hVDAC2 barrel; DPPC lies between DMPC and DSPC. The barrel structure is colored based on the protein stability (deduced from experimental measurements and from barrel plasticity values obtained from MDS), with the most favorable condition represented in green and the least favorable condition represented in red. Of the three lipid conditions, DPPC provides optimal negative mismatch that stabilizes hVDAC2 barrel.

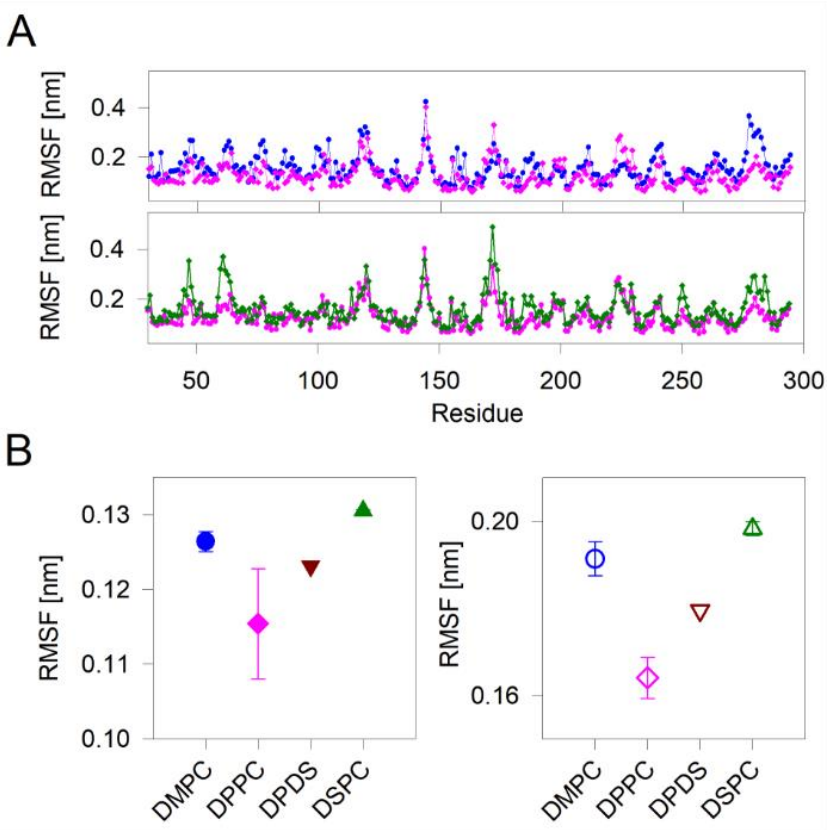

Figure S6. hVDAC2 RMSF in various lipid conditions. (A) Comparison of per-residue RMSF by overlaying DMPC–DPPC system (upper panel) and DPPC–DSPC system (lower panel). Color codes used are: DMPC in blue, DPPC in pink and DSPC in green. (B) Average per residue RMSF for the strand residue (left) and for the loop residue (right) is shown (DPDS is in brown). Error bar represents standard deviation of two independent 200 ns simulations.

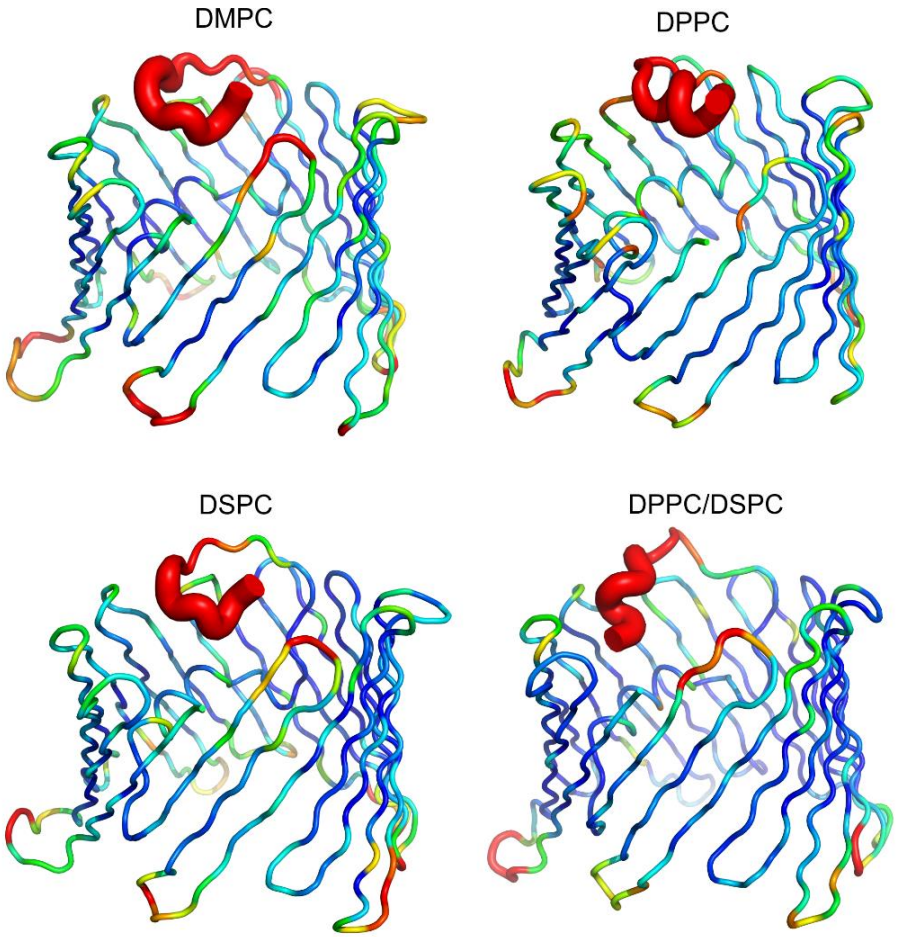

Figure S7. Sausage representation of hVDAC2 from the MDS in PC lipids. Shown here are the results from DMPC, DPPC, DSPC and DPPC/DSPC (DPDS) bilayer systems. DPPC shows the least fluctuation in the loop region. Further, the N-terminal extension is more structured in DPPC among all the lipid conditions. The extent of fluctuation seen is represented using the color gradient from blue (low fluctuation, LF) to red (high fluctuation, HF).

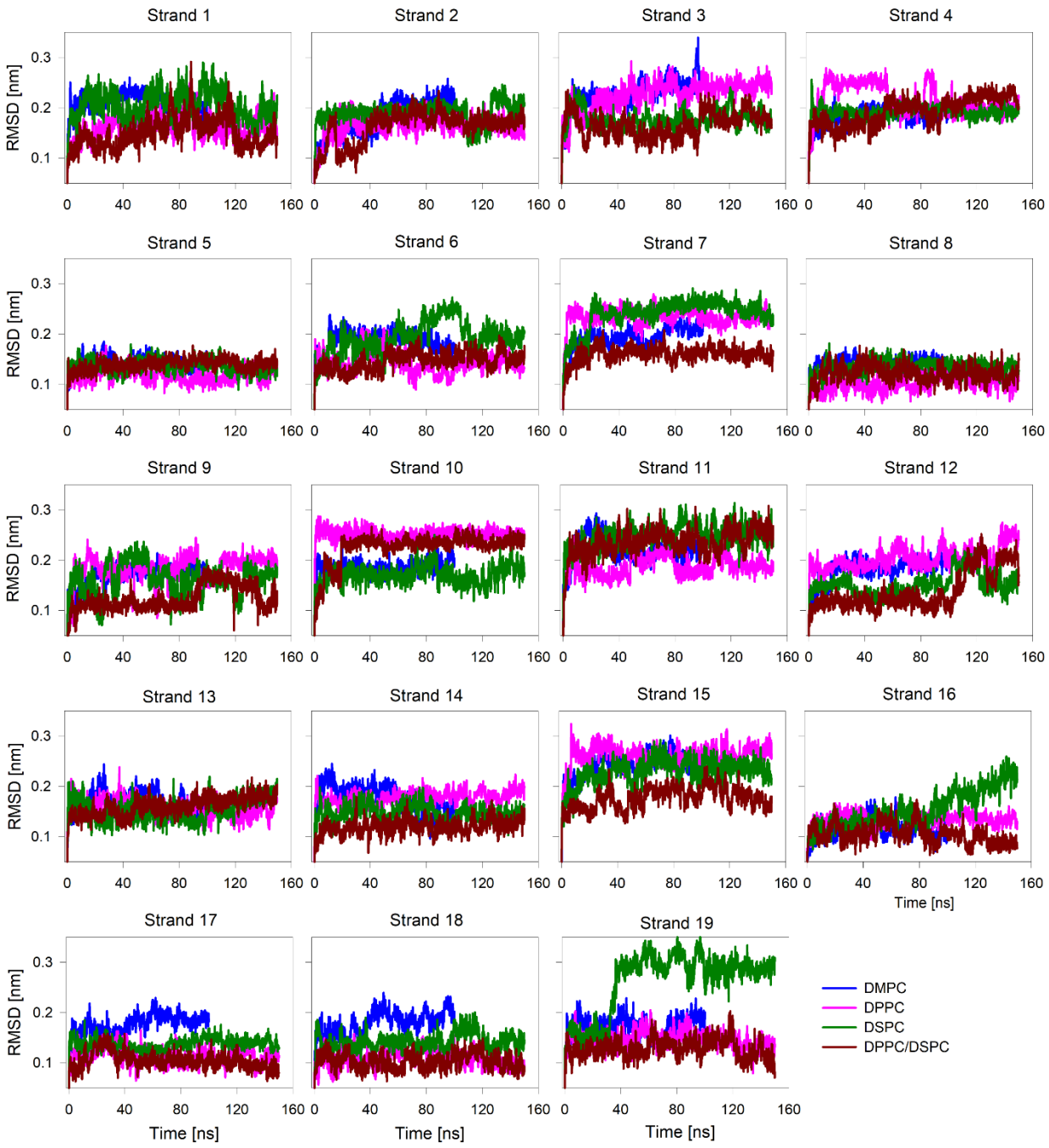

Figure S8. RMSD derived from all-atom MDS in lipids for hVDAC2. Shown here is the overlay of RMSD derived for every strand of hVDAC2 for all four lipidic bilayer system from 0-100/150 ns simulation trajectory. Color scheme used for each lipid is provided in the bottom right corner. The observed trend in the overall RMSD for the strands follows the order DPPC/DSPC < DPPC < DSPC < DMPC. While the RMSD for strands 10 and 15 are highest in DPPC, the overall RMSD of the entire protein (both strand and loop RMSD) is lowest in DPPC.

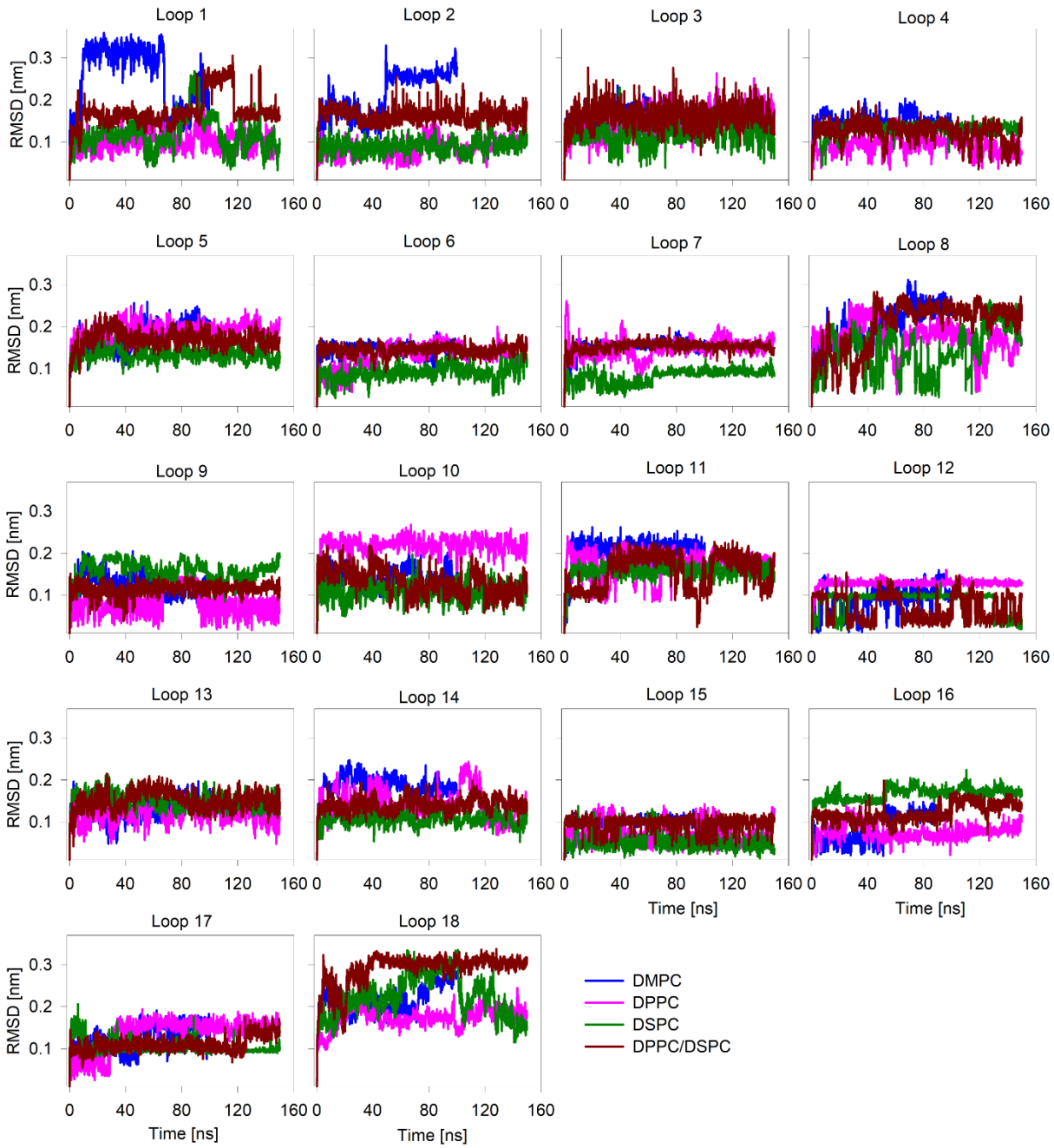

Figure S9. RMSD derived from all-atom molecular dynamics simulations in lipids for hVDAC2. Shown here is the overlay of RMSD derived for every loop region of hVDAC2 for all four lipid bilayer systems from 0-100/150 ns simulation trajectory. Color scheme used for each lipid is provided in the bottom right corner. The observed trend in RMSD follows the order DSPC < DPPC < DMPC < DPPC/DSPC, and the overall RMSD of the entire protein (both strand and loop RMSD) is lowest in DPPC. For example, when we compare DPPC and DMPC, the RMSD of only three loops, namely 9, 11 and 13, is higher in DPPC, while it is lower in the other fifteen loop regions. Similarly, compared with DSPC, only loops 7 and 13 exhibit higher fluctuation in DPPC, and the dynamics is lower in all other loops.

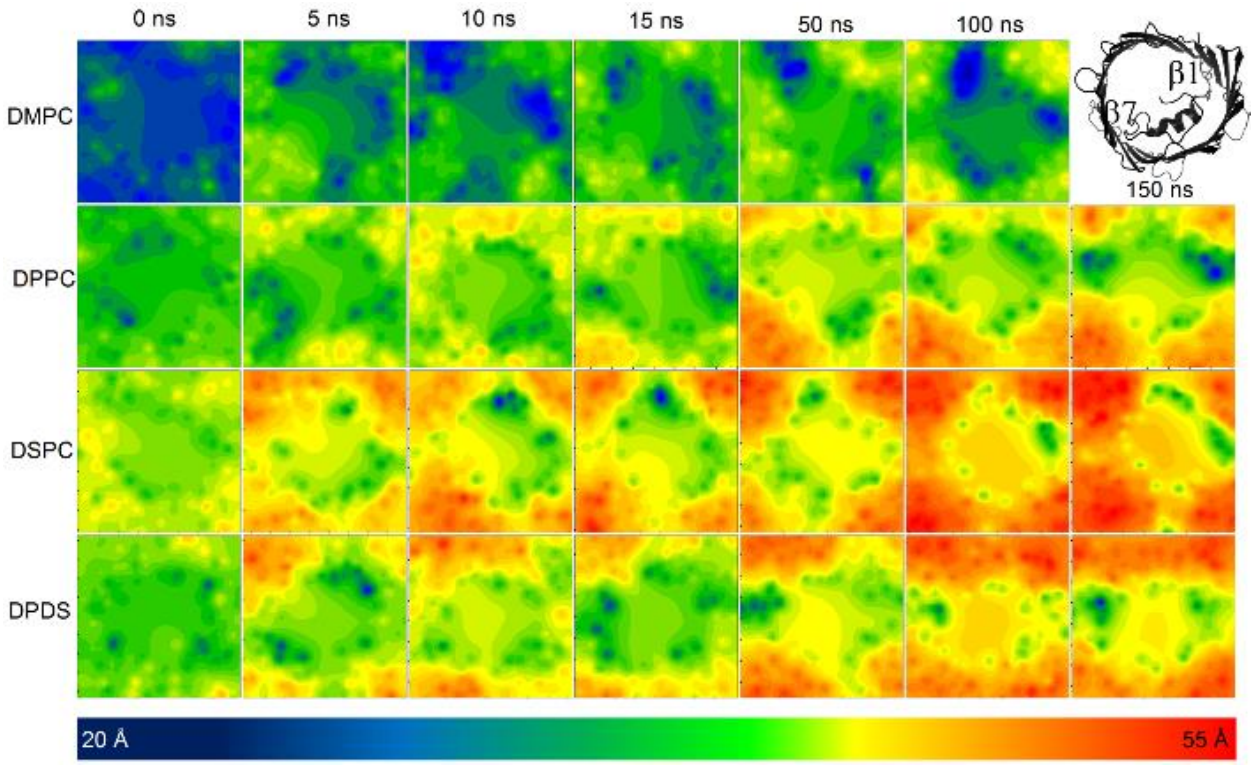

Figure S10. Lipid redistribution and change in membrane thickness with simulation time. Representative lipid thickness maps obtained from MEMBPLUGIN v1.1 (5) at 0, 5, 10, 15, 50, 100, and 150 ns of the simulation trajectory for all four lipid bilayers (DMPC, DPPC, DSPC, DPPC/DSPC (DPDS)). Each square is a two-dimensional representation of the simulation box. As the simulation progresses, we see a clear change in the bilayer thickness map, with thinning and thickening of specific membrane regions. The hVDAC2 barrel orientation was common in each bilayer thickness map, and is shown as a schematic (right top corner). The color scale and the corresponding lipid thickness range are provided below the composite image. Note that there is a known bug in the MEMBPLUGIN software, which calculates densities within the barrel, although no lipid is present (5). Hence, the lipid thickness map is only to be interpreted qualitatively.

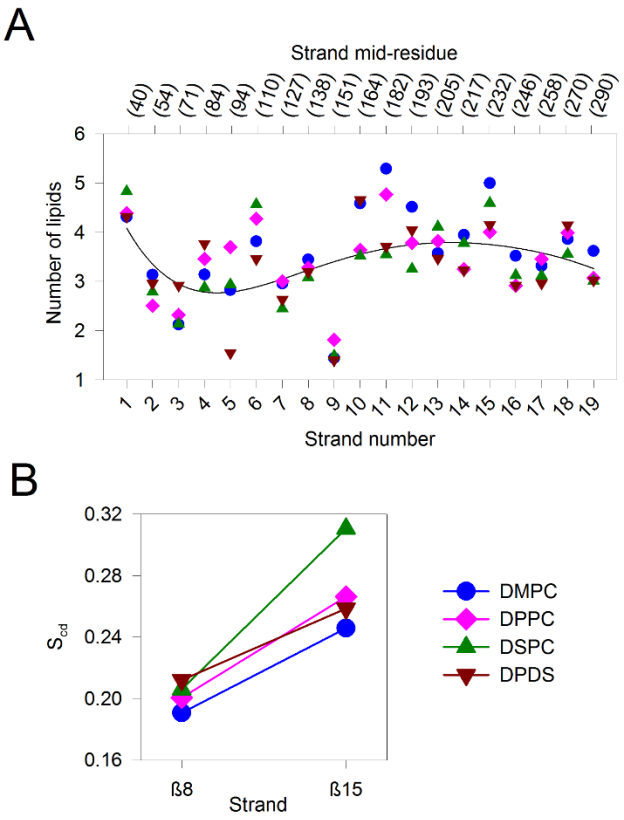

Figure S11. Asymmetric membrane thinning near specific barrel segments. (A) The number of lipid molecules (*y* axis) calculated in the 5 Å vicinity of the lipid-facing midplane residue of each strand (upper *x* axis) and for the complete strand (lower *x* axis) using the VMD TK-console script, is plotted here. The results show regions of the barrel where membrane thinning is evident (fewer lipid molecules) in all four lipid conditions (DMPC, DPPC, DSPC and DPPC/DSPC (DPDS)). The regression line is provided as a visual guide for the overall variation in lipid number across the hVDAC2 barrel. (B) Comparison of the lipid order parameter (S_{cd}) calculated for the mid residue of 8^{th} (membrane thinning region) and 15^{th} (membrane thickening region) strand. Lipid molecules in the 10 Å vicinity were used for the calculation. As expected, the S_{cd} is lowered near the 8^{th} strand, which supports membrane thinning in this region (note that membrane thinning creates lipid deformation and lowers the S_{cd}). S_{cd} is high near the 15^{th} strand where we see lipid thickening in all four lipid conditions.

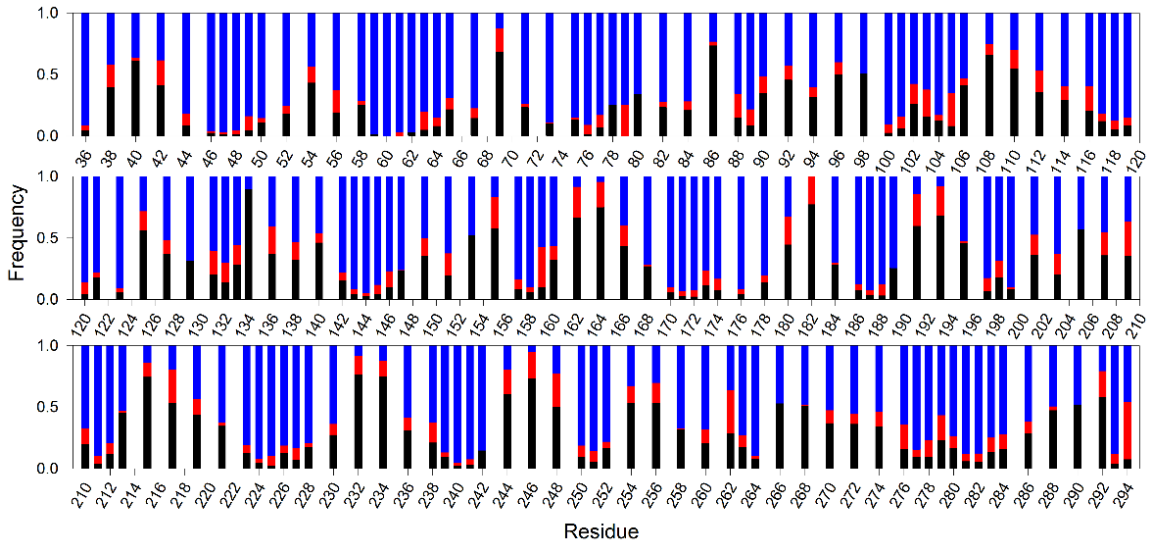

Figure S12. Vicinity analysis in hVDAC2-DMPC system. Frequency of occurrence each surrounding molecule (water, blue; lipid headgroup (P-atom), red; lipid hydrocarbon chain, black) near the 5 Å vicinity of all lipid facing strand residues, and all loop residues of hVDAC2 is plotted for DMPC bilayer system. Strand midplane residues are buried, and therefore show greater frequency of lipid acyl chain atoms. Similarly, interface and loop residues show greater occupancy of water and lipid head group in their vicinity.

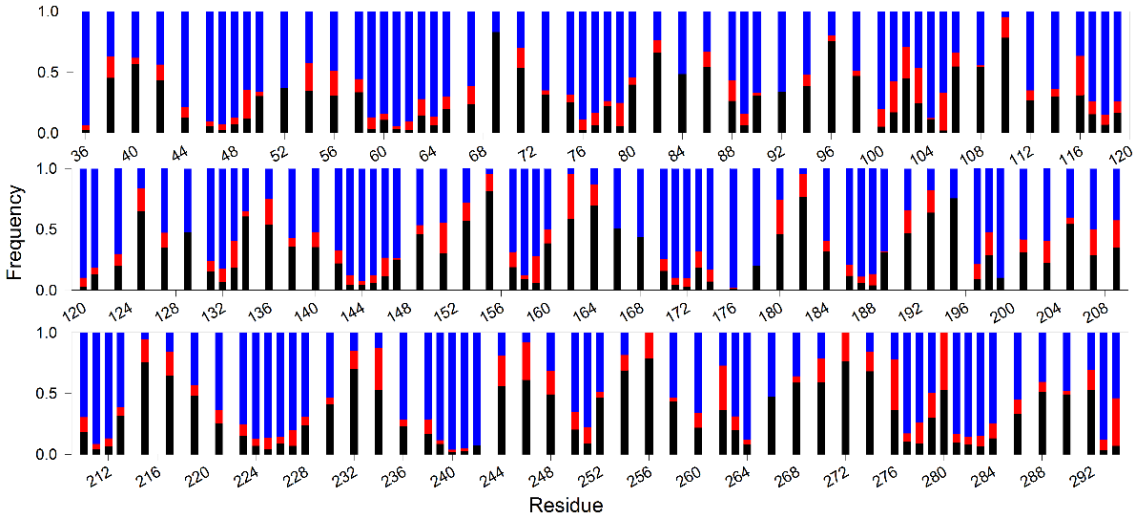

Figure S13. Vicinity analysis in hVDAC2-DPPC system. Frequency of occurrence each surrounding molecule (water, blue; lipid headgroup (P-atom), red; lipid hydrocarbon chain, black) near the 5 Å vicinity of all lipid facing strand residues, and all loop residues of hVDAC2 is plotted for DPPC bilayer system. Strand midplane residues are buried, and therefore show greater frequency of lipid acyl chain atoms. Similarly, interface and loop residues show greater occupancy of water and lipid head group in their vicinity.

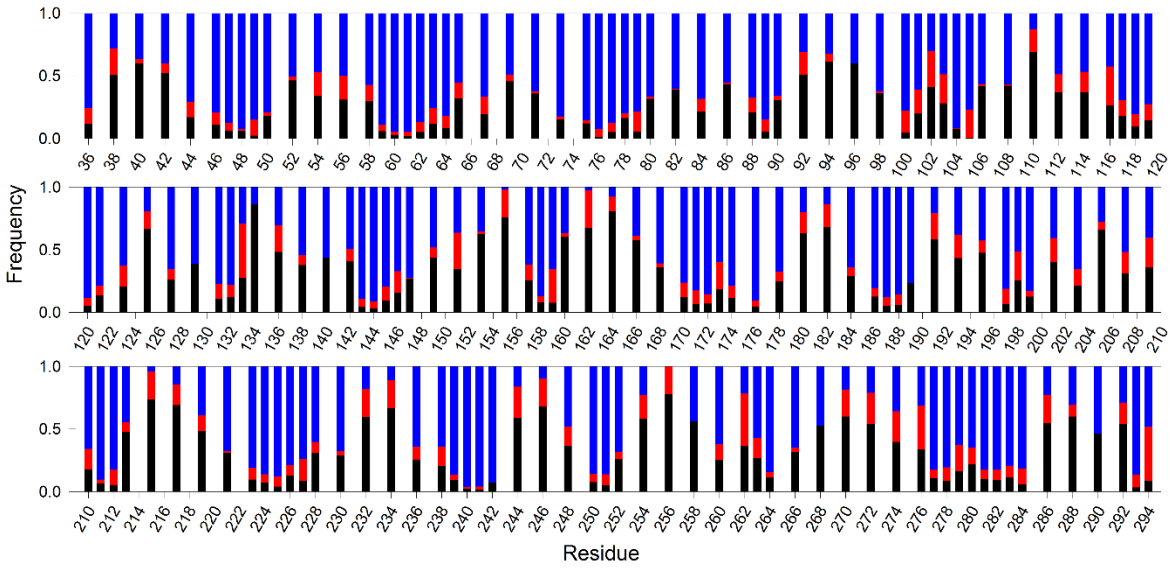

Figure S14. Vicinity analysis in hVDAC2-DSPC system. Frequency of occurrence each surrounding molecule (water, blue; lipid headgroup (P-atom), red; lipid hydrocarbon chain, black) near the 5 Å vicinity of all lipid facing strand residues, and all loop residues of hVDAC2 is plotted for DSPC bilayer system. Strand midplane residues are buried, and therefore show greater frequency of lipid acyl chain atoms. Similarly, interface and loop residues show greater occupancy of water and lipid head group in their vicinity.

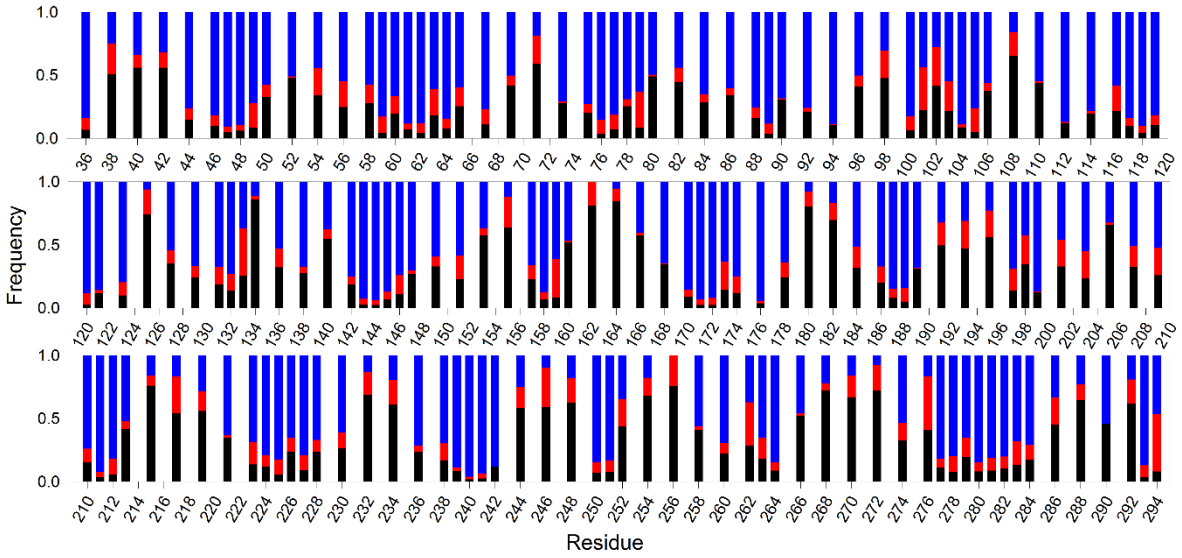

Figure S15. Vicinity analysis in hVDAC2-DPDS system. Frequency of occurrence each surrounding molecule (water, blue; lipid headgroup (P-atom), red; lipid hydrocarbon chain, black) near the 5 Å vicinity of all lipid facing strand residues, and all loop residues of hVDAC2 is plotted for the DPPC/DSPC bilayer system. Strand midplane residues are buried, and therefore show greater frequency of lipid acyl chain atoms. Similarly, interface and loop residues show greater occupancy of water and lipid head group in their vicinity.

Figure S16. Comparison of barrel deformation in various lipid bilayers. The hVDAC2 structures derived from 10 frames between the 50–100 ns simulation trajectory was averaged, and is shown here using the cartoon representation. Barrel structures in DMPC (top left, blue), DSPC (top right, green) and DPDS (bottom, brown) are overlaid here individually with the average structure in DPPC (pink). Overall, DPPC shows less deformation, while deformation of strands β3-β6 (shown as magnified image) is more pronounced in the other three lipids, particularly in DMPC.

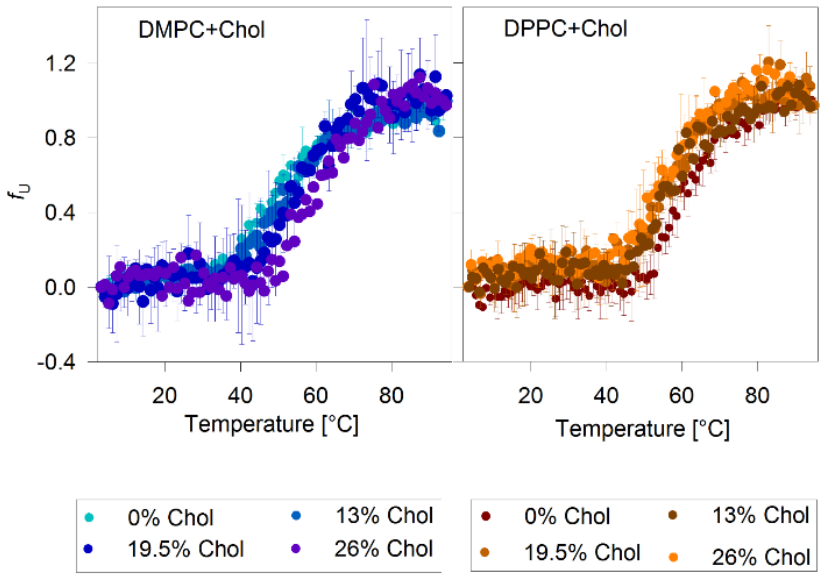

Figure S17. Effect of increasing cholesterol and acyl chain length on hVDAC2 stability. Dependence of the unfolded protein fraction (f_U) on temperature, derived from far-UV CD thermal unfolding at 215 nm is plotted here for q = 1.0 DMPC bicelles (left) and DPPC bicelles (right) with increasing cholesterol percentage. Color guides for both panels are shown below the plot. Error bars represent the s. d. calculated from 2-3 independent datasets. Data for DSPC:DPC bicelles is not shown here, as bicelles with higher percentages of cholesterol could not be prepared.

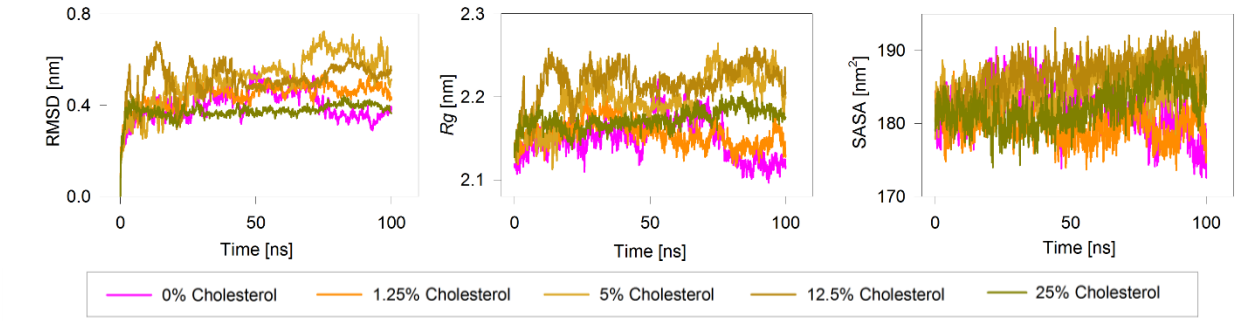

Figure S18. Parameters derived from all-atom molecular dynamics simulations in DPPC for hVDAC2 with increasing (0-25%) cholesterol content. Root mean square deviation (RMSD), radius of gyration (R_g) and solvent accessible surface area (SASA) derived for the full-length protein from the 100 ns simulations. The color/ symbol used for each condition is presented below the figure. RMSD for 0% cholesterol (pink line) and 25% cholesterol (green line) are comparable while it is higher in other cholesterol conditions. R_g and SASA do not show any significant change.

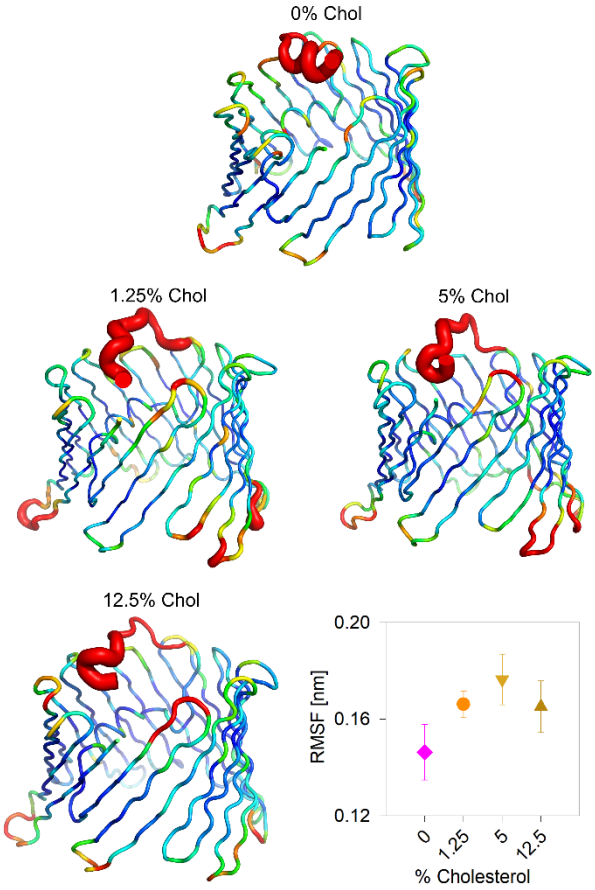

Figure S19. Sausage representation of hVDAC2 from the 100 ns MD simulations in DPPC bilayers with increasing cholesterol percentage. Shown here are the results from 0%–12.5% cholesterol (abbreviated as Chol). DPPC containing no cholesterol (0% Chol) shows the least fluctuation in the loop region. Further, the N-terminal extension is more structured in this condition. The extent of fluctuation seen is represented using the color gradient from blue (low fluctuation) to red (high fluctuation). Also shown is the plot of total RMSF with increasing cholesterol % (bottom right).

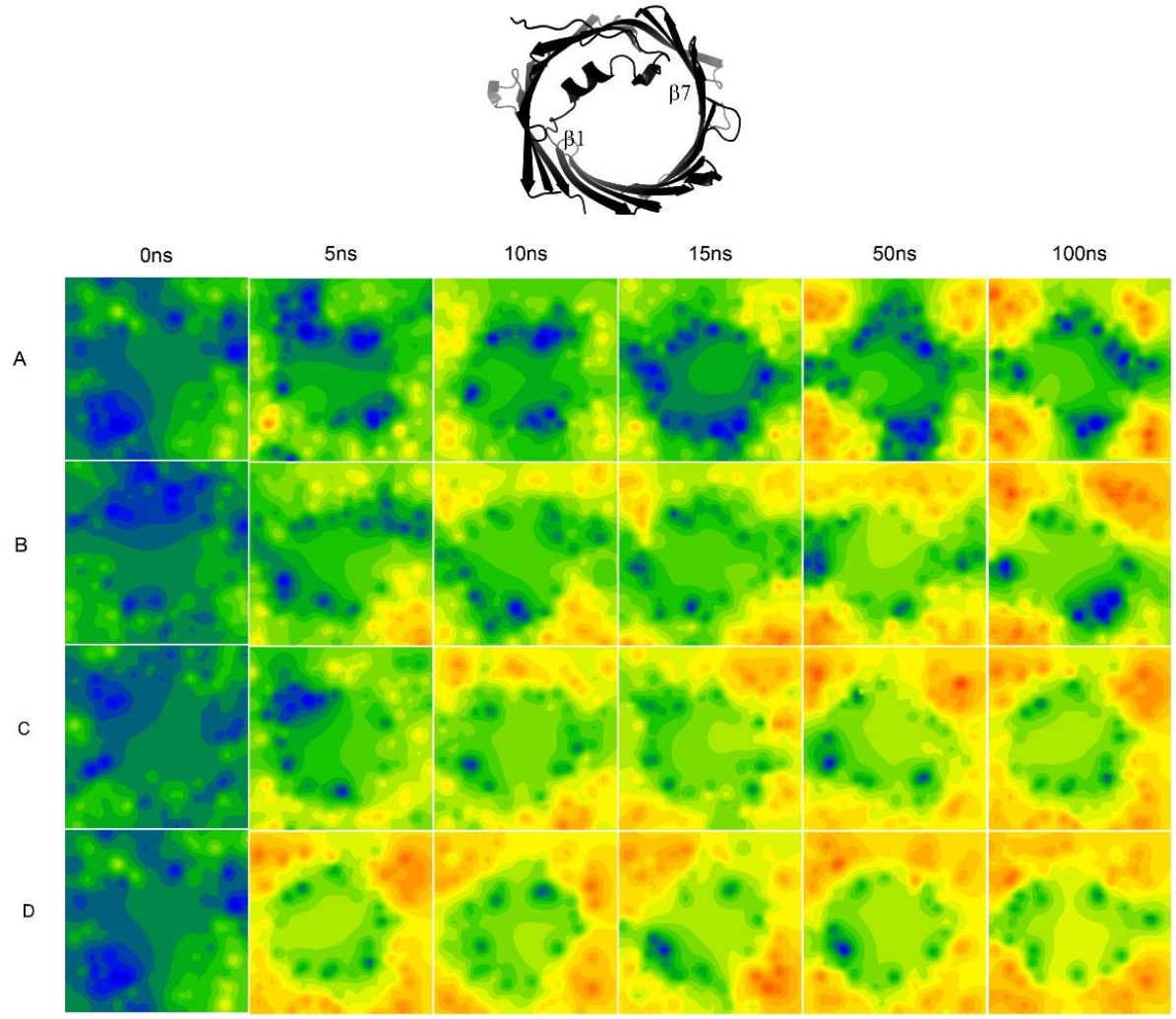

Figure S20. Lipid redistribution and change in membrane thickness with simulation time. Representative lipid thickness maps obtained from MEMBPLUGIN v1.1 (5) at 0, 5, 10, 15, 50, and 100 ns of the simulation trajectory for DPPC bilayers with increasing cholesterol content ((A) 1.25%, (B) 5%, (C) 12.5%, (D) 25% cholesterol). Each square is a two-dimensional representation of the simulation box. As the simulation progresses, the magnitude of change in the thickness map from the starting frame of the simulation to the last frame decreases with increasing cholesterol content. Hence, the membrane dynamicity is lowered when the cholesterol content of the DPPC bilayer increases. The hVDAC2 barrel orientation was common in each bilayer thickness map, and is shown as a schematic (top). The color scale and the corresponding lipid thickness range used in Figure S10 are retained here.

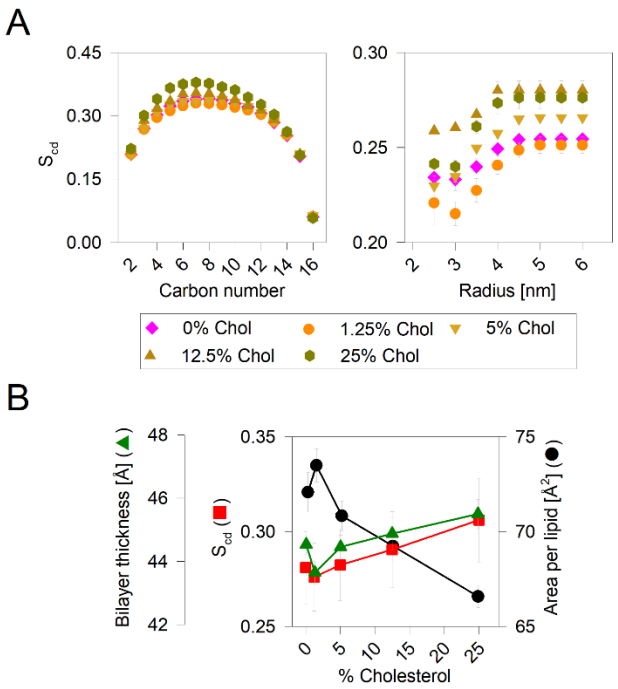

FIGURE S21. Effect of hVDAC2 on the DPPC bilayer physical property with increasing cholesterol content. (A) Bilayer S_{cd} was derived for 10 frames from 50–100 ns trajectory of the 100 ns MD simulation. Color/ symbol guide for the various cholesterol percentages is shown below plot (A). (Left) Average S_{cd} values for all 10 frames are plotted for each acyl carbon. As anticipated, the S_{cd} increases with increasing cholesterol content. (Right) Change in S_{cd} with distance from the hVDAC2 barrel center. S_{cd} is lowest near the protein, as protein creates deformation in the lipid membrane. (B) Average S_{cd}, APL and bilayer thickness derived from 10 frames of the 50–100 ns trajectory for the various cholesterol conditions. A prominent decrease in APL (black circle) is seen, while the S_{cd} (red squares) and bilayer thickness (green upward triangle) increases marginally.

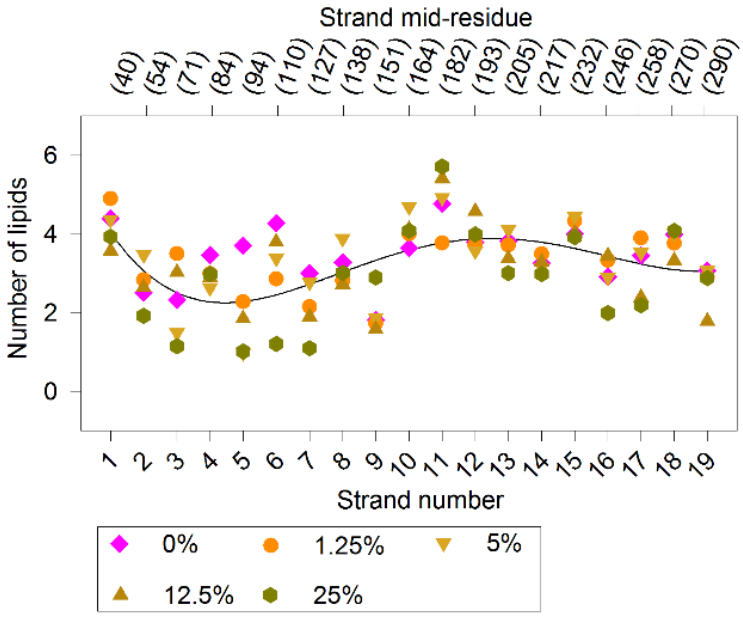

Figure S22. Asymmetric membrane thinning near specific barrel segments is retained in cholesterol with concomitant lowering in number of vicinal lipids. The number of lipid molecules (y-axis) calculated in the 5 Å vicinity of the lipid-facing midplane residue of each strand (upper x-axis) and for the complete strand (lower x-axis) using the VMD TK-console script, is plotted here. With increasing cholesterol content, the number of lipid molecules in the vicinity of strands β3-β7 is lowered compared to without cholesterol (0%). The regression line is provided as a visual guide for the overall variation in lipid number across the hVDAC2 barrel. Color/ symbol guide for the various cholesterol percentages is shown below the plot.

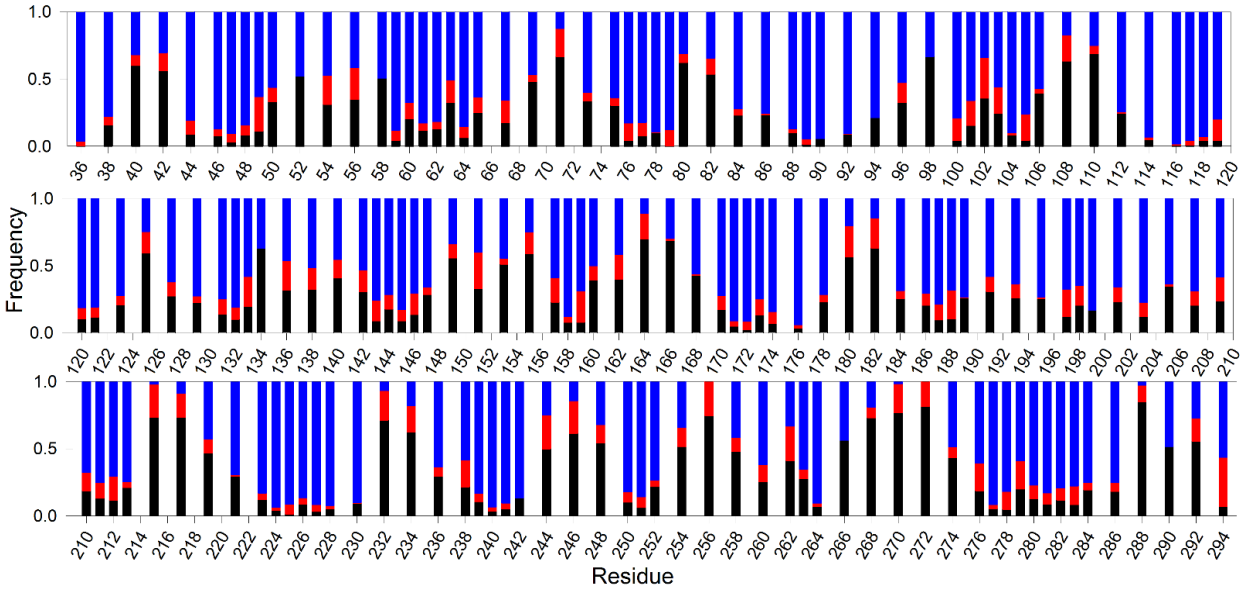

Figure S23. Vicinity analysis in hVDAC2-DPPC-1.25% cholesterol system. Frequency of occurrence each surrounding molecule (water, blue; lipid headgroup (P-atom), red; lipid hydrocarbon chain, black) near the 5 Å vicinity of all lipid facing strand residues, and all loop residues of hVDAC2 is plotted for DPPC-1.25% cholesterol bilayer system. Strand midplane residues are buried, and therefore show greater frequency of lipid acyl chain atoms. Similarly, interface and loop residues show greater occupancy of water and lipid head group in their vicinity.

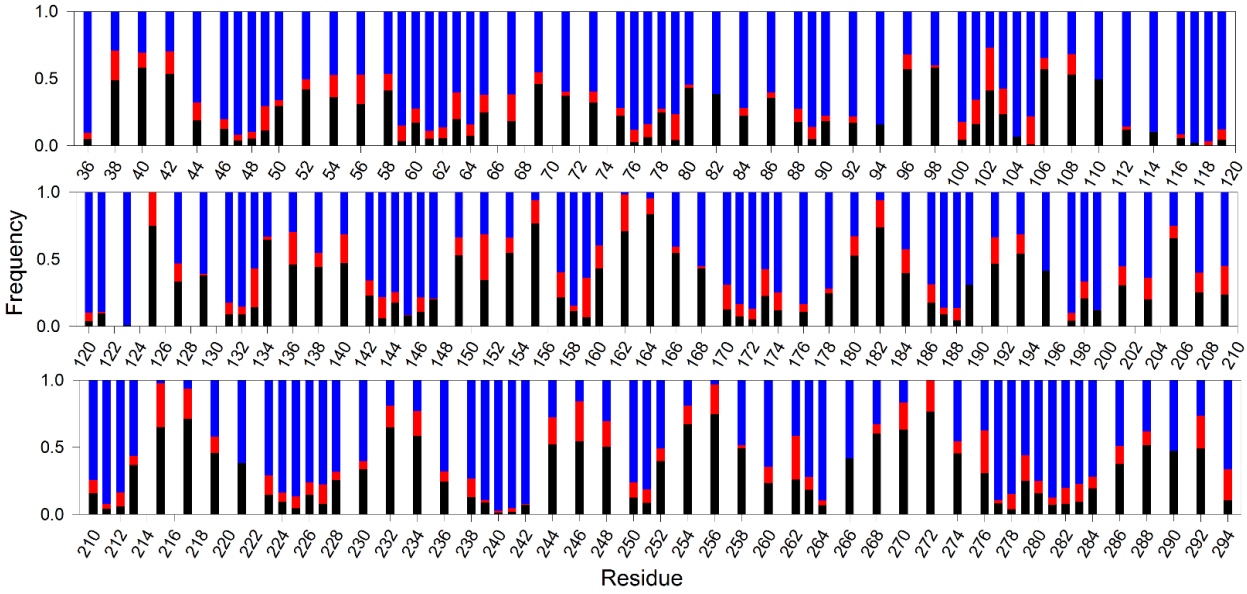

Figure S24. Vicinity analysis in hVDAC2-DPPC-5.0% cholesterol system. Frequency of occurrence each surrounding molecule (water, blue; lipid headgroup (P-atom), red; lipid hydrocarbon chain, black) near the 5 Å vicinity of all lipid facing strand residues, and all loop residues of hVDAC2 is plotted for DPPC-5% cholesterol bilayer system. Strand midplane residues are buried, and therefore show greater frequency of lipid acyl chain atoms. Similarly, interface and loop residues show greater occupancy of water and lipid head group in their vicinity.

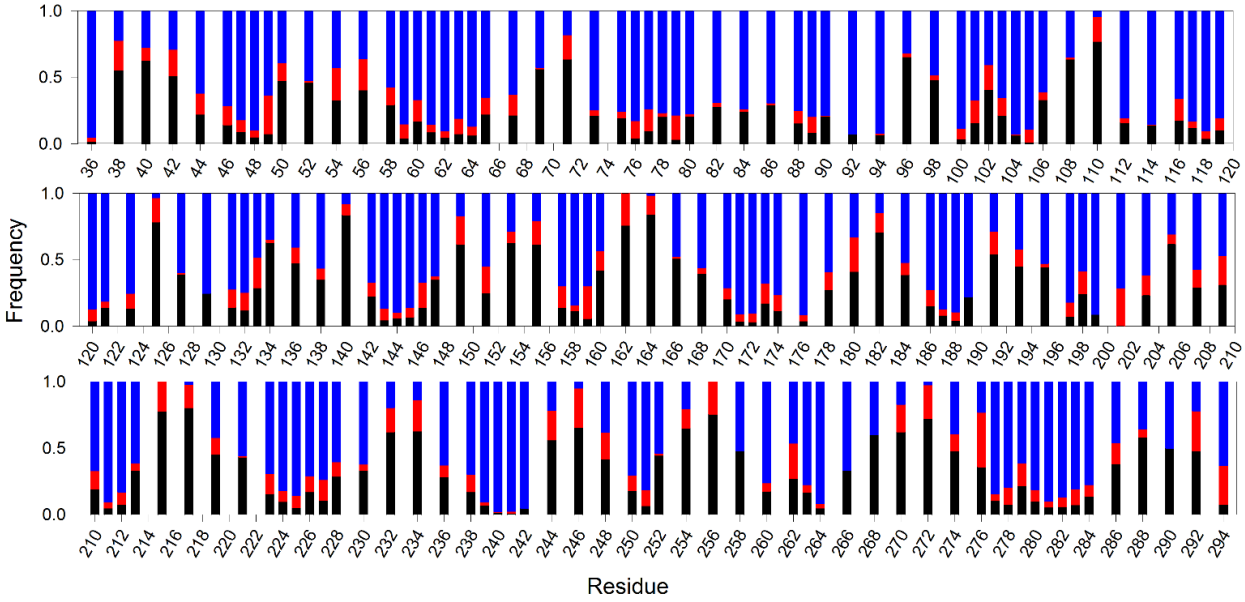

Figure S25. Vicinity analysis in hVDAC2-DPPC-12.5% cholesterol system. Frequency of occurrence each surrounding molecule (water, blue; lipid headgroup (P-atom), red; lipid hydrocarbon chain, black) near the 5 Å vicinity of all lipid facing strand residues, and all loop residues of hVDAC2 is plotted for DPPC-12.5% cholesterol bilayer system. Strand midplane residues are buried, and therefore show greater frequency of lipid acyl chain atoms. Similarly, interface and loop residues show greater occupancy of water and lipid head group in their vicinity.

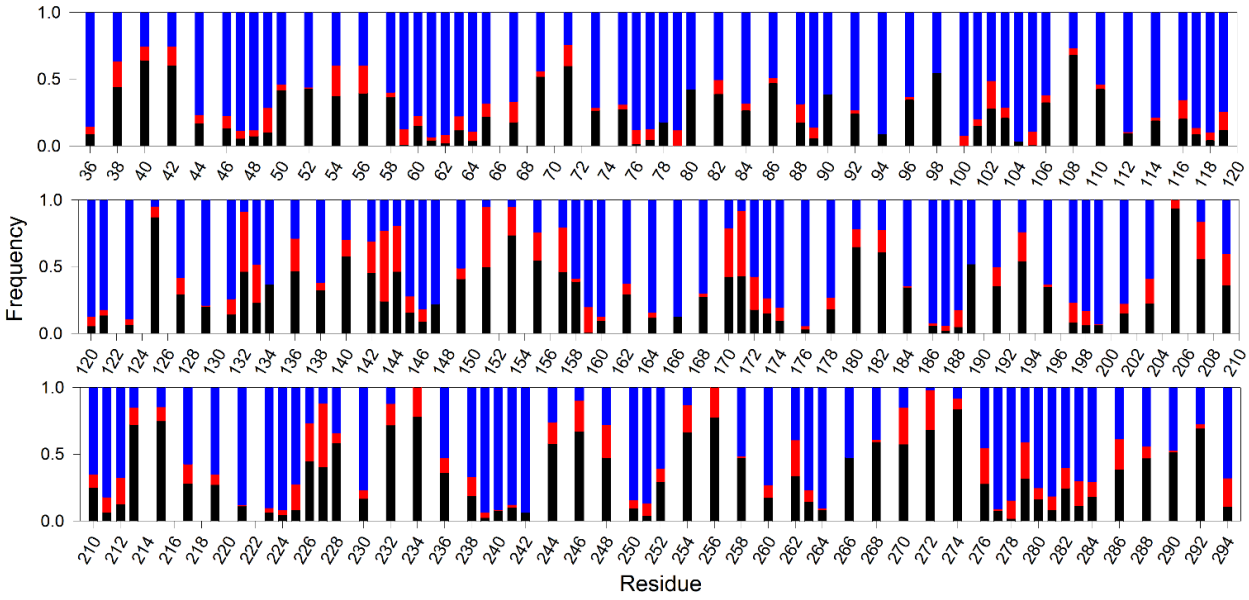

Figure S26. Vicinity analysis in hVDAC2-DPPC-25.0% cholesterol system. Frequency of occurrence each surrounding molecule (water, blue; lipid headgroup (P-atom), red; lipid hydrocarbon chain, black) near the 5 Å vicinity of all lipid facing strand residues, and all loop residues of hVDAC2 is plotted for DPPC-25% cholesterol bilayer system. Strand midplane residues are buried, and therefore show greater frequency of lipid acyl chain atoms. Similarly, interface and loop residues show greater occupancy of water and lipid head group in their vicinity.

SUPPORTING CITATIONS

1. Kucerka, N., M. P. Nieh, and J. Katsaras. 2011. Fluid phase lipid areas and bilayer thicknesses of commonly used phosphatidylcholines as a function of temperature. *Biochim. Biophys. Acta* 1808:2761-2771.
2. Maurya, S. R., and R. Mahalakshmi. 2013. Modulation of human mitochondrial voltage-dependent anion channel 2 (hVDAC-2) structural stability by cysteine-assisted barrel-lipid interactions. *J. Biol. Chem.* 288:25584-25592.
3. Maurya, S. R., and R. Mahalakshmi. 2015. N-helix and Cysteines Inter-regulate Human Mitochondrial VDAC-2 Function and Biochemistry. *J. Biol. Chem.* 290:30240-30252.
4. Silvius, J. R. 1982. Thermotropic Phase Transitions of Pure Lipids in Model Membranes and Their Modifications by Membrane Proteins. In Lipid-Protein Interactions. P. C. Jost, and O. H. Griffith, editors. John Wiley & Sons, Inc., New York. 239-281.
5. Guixa-Gonzalez, R., I. Rodriguez-Espigares, J. M. Ramirez-Anguita, P. Carrio-Gaspar, H. Martinez-Seara, T. Giorgino, and J. Selent. 2014. MEMBPLUGIN: studying membrane complexity in VMD. *Bioinformatics* 30:1478-1480.